The use of digital twins to remotely update feedback controllers for the motion control of nonlinear dynamic systems

Yoav Vered[a] and Stephen J. Elliott[b]

Institute of Sound and Vibration Research, University of Southampton, SO17 1BJ, United Kingdom

Preprint version.

Published at Mechanical Systems and Signal Processing

volume 185, 15 February 2023, doi: https://doi.org/10.1016/j.ymssp.2022.109770

Keywords: Digital twin; Adaptive control; Reconfigurable feedback controller; Backlash; Dead zone controller.

---

[a] Electronic mail: V.Yoav@soton.ac.uk

[b] Electronic mail: S.J.Elliott@soton.ac.uk

The use of a digital twin to update a feedback controller is considered, and this is illustrated using simulations of a position-controlled dynamical system with a time-varying nonlinear element. The feedback control system consists of a dc motor driving the displacement of a three degree of freedom structure through a lead screw that is subject to backlash, whose gap angle changes over time due to wear for example. The backlash is shown to destabilise the feedback loop when using a PID controller designed for the linear system. However, stability can then be re-established by including a dead zone within the controller. The design of the dead zone depends on the extent of the gap angle in the backlash and is a trade-off between stabilising the system and avoiding excessive steady-state errors and undesired transient behaviour. When the backlash gap angle changes significantly from the one used to design the dead zone, both performance and stability are affected. Therefore, a digital twin of the system is used to estimate the backlash gap angle as it changes with time and this estimate is used to re-design the dead zone, which is then communicated back to update the controller. The digital twin and controller-design process can be implemented offline and remotely from the physical twin and the real-time controller via an asynchronous link with variable time delays. As a result of combining the feedback loop and digital twin, good performance and stability are maintained at all times.

1. Introduction

If a mechanical system is controlled using feedback, but its characteristics change over time, the original design of a feedback controller may not perform well and may even become unstable [1]. It is thus important to be able to monitor the condition of the mechanical system so that the control strategy can be modified in response to these changes. In this paper, the use of a digital twin [2] is investigated to track the behaviour of the mechanical system under control, which comprises the physical twin. The digital twin is then used to re-design the feedback controller, as illustrated in Figure 1.

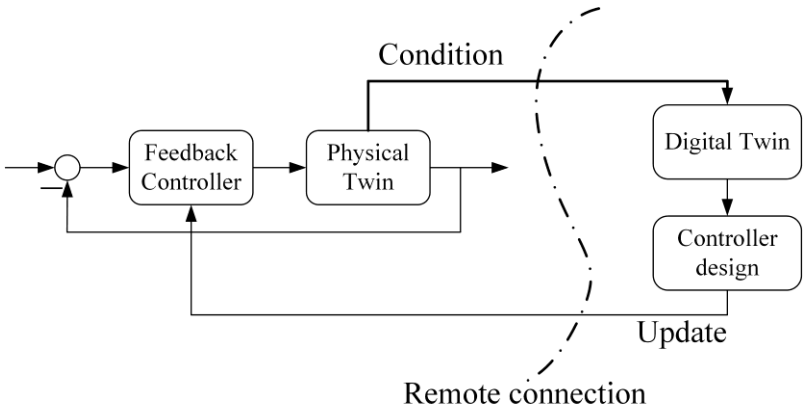

Figure 1 – A reconfigurable motion feedback controller design based on a digital twin framework.

Although the feedback controller for the physical system must act in real-time, and so generally is implemented locally, the implementation of the digital twin and the re-design of the controller need not be performed so quickly and so could be implemented remotely, via an internet connection with an uncertain delay for example. This general idea is illustrated in this paper based on a servomechanism in which the difference between the measured position of a structure and a reference command signal is used to drive a feedback controller to reduce this difference, hence ensuring the position of the structure follows the reference signal. Servomechanisms are widely used in the aviation industry to control the position of flight surfaces, for example [3], and in wind turbines to control the pitch of the blades [4]. When the control settling time is close to the structure's fundamental vibration period time, the structure under control can

exhibit significant dynamic behaviour. The servomechanism is initially designed to control the position of a dynamic (flexible) structure when it is linear, but which then needs to be re-designed if the physical system becomes increasingly nonlinear over time, for example, due to wear. Although backlash, to some degree, is present in most mechanical position control systems [5], its effect on the linear feedback law is frequently neglected. However, even when the backlash is considered when formulating the identification and control problem [6,7], its characteristics are usually modelled as constant in time. This form of modelling may be applicable in some cases, but it is not suitable when wear and tear processes occur [6], in which case the characteristics of the backlash can change over time [8]. A possible method to account for the time dependence of the backlash is by introducing an adaptive controller [7], which estimates the backlash as part of its loop. In [9], an inverse-backlash adaptive control algorithm is described that estimates the backlash parameters in real-time. However, this proposed solution is only valid when the backlash can be measured directly and instantaneously, meaning that there is no inertia between the command signal and the backlash. In the review [7], it is suggested that in cases where the backlash is sandwiched between two dynamical systems, it is better to use a linear controller without the inverse backlash compensation. Other solutions for the so-called backlash sandwich problem have been introduced in the literature, either by employing nonlinear adaptive control [10], model predictive control [11], sliding mode control [12], or neural networks [13].

The drawback of such methods is that the controllers' structures are complex, and their implementation is not direct. Therefore, although the theory behind these methods may be well understood, they are not industry-friendly, and in practice, linear PID controllers are still dominant [14].

At its core, the purpose of a digital twin is to create a fusion between physical and data-based models of a system. Each of these modelling techniques are separately well understood; see [15,16] for physical-based modelling and [17,18] and references therein for data-based models. The technology maturity in computing power and sensor embedding needed to realise a digital twin was only recently made possible [2]. The majority of the work in this area is concerned with digital twins use for decision-making and

structural health monitoring, with only a few remarks on the use of digital twins in control, using classical ideas like controller scheduling [19]. Developments in digital signal processing have, however, given rise to a more profound understanding of advanced control methodologies [20–22]. Therefore, the question of how best digital twins can be used for autonomous control is still open. This work focuses on how the digital twin can be employed in feedback position control. The full capabilities or scope of the digital twin framework is not discussed. Instead, reference [2] is suggested for additional details on digital twin and their multiple uses for engineering dynamical systems.

A simulation of a servomechanism is being used in this work to demonstrate the use of the digital twin, based on the architecture of Figure 1. The dynamical structure is modelled here using a simple three degree-of-freedom (DOF) system of the form previously studied in [23]. A dc motor is used to drive the structure via a lead screw, which is assumed to be subject to a time-varying backlash of unknown magnitude. The structure is being controlled using a linear PID controller, with the incorporation of a dead zone to overcome the limit cycles introduced by the backlash and keep the control effort minimal in the backlash gap [7]. The dead zone parameter is estimated asynchronously by using a remotely-based digital twin to monitor the changing backlash angle. The initial simulation study described here aims to demonstrate the capabilities of incorporating digital twins into system control by employing the digital twin as an asynchronous estimator, resulting in a simple structure of the digital controller. This idea is not, by any means, a demonstration of the full capabilities of digital twins but only acts as a stepping stone towards a fuller understanding of their potential use in feedback control.

The structure of the paper is that Section 2 describes the model of the linear physical system and its control, Section 3 considers the effect of backlash on the feedback controller, and Section 4 illustrates the closed-loop identification of the backlash and its use in a digital twin to re-design the feedback controller.

2. Linear control of the physical twin

In this paper, the servomechanism is designed for the position control of a three DOF structure, as shown in Figure 2(a). The bottom mass of the structure is connected to a dc electromechanical motor via a lead screw. A simplified dynamic system model can be derived using lumped elements, as shown in Figure 2(b).

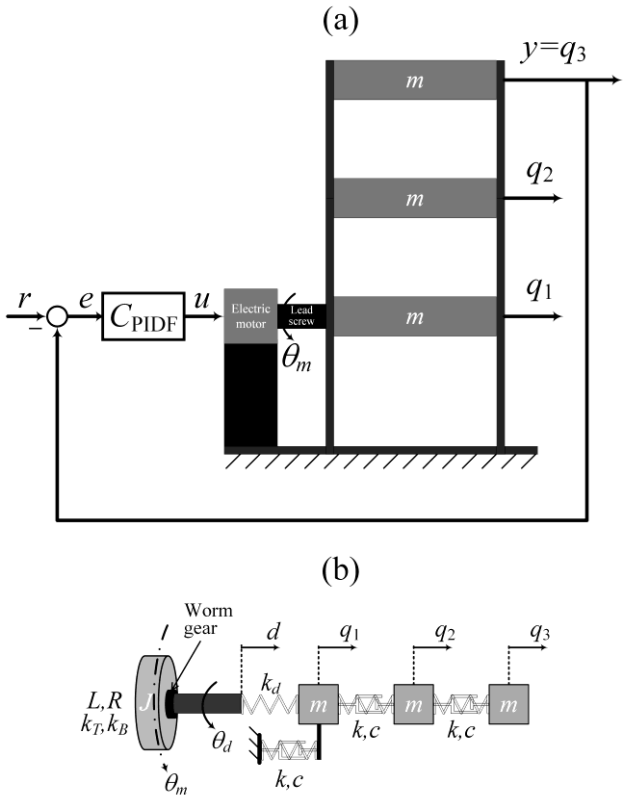

Figure 2 – The model of the simulated three DOF system with a simple position feedback control system (a), and the electromechanical system's lumped element model (b).

The dc motor electrical model parameters are its inductance, L, and resistance, R, it is modelled as a lumped inertia, J, the two motor's coefficients, k_T and k_B are the torque and back-emf gains, and the motor angular velocity and position are denoted ω_m and θ_m, respectively. The three DOF structure is modelled as three equal lumped masses, each of mass m, connected in series via linear springs, k, and linear dampers, c. The lead screw is connected to the motor via a worm gear with a 1:1 gear ratio. Its angular position is denoted

as θ_d and its elongation (from rest) is denoted as d such that $d = p\theta_d$, where θ_d is in radians, and p is the pitch of the lead screw. The lead screw connection to the first platform can be modelled as a linear spring k_d, although this is assumed to be very large in the simulations below. The absolute position of each of the structure's platforms are denoted q_i $(i = 1,2,3)$. The worm gear is susceptible to developing backlash, however, and so the motor's angle, θ_m, does not necessarily equal to the lead screw's angle, θ_d.

2.1. Linear model derivation

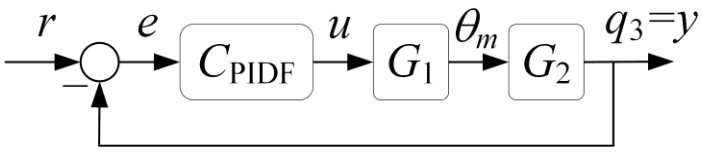

Figure 3 – Linear feedback control block diagram.

In this section, the linear models are described based on the lumped model of Figure 2(b) with no backlash. The feedback control block diagram is shown in Figure 3, in which G_1 and G_2 denote the dynamic plant responses associated with the electric motor and the 3 DOF system, respectively, and C_{PIDF} denotes a linear PID controller, as discussed below. The reference, or command signal, is denoted r, y is the output signal, which corresponds to the position of the top mass in this case, e the tracking error signal, and u the voltage control signal.

In the derivation of the linear models, the following assumptions are used:

- The inertial loading of the structure is negligible compared to the motor's torque.
- The lead screw is infinitely rigid, i.e., $k_d \to \infty$.
- The worm gear does not have any backlash, i.e., $\theta_d = \theta_m$.

The dc motor's dynamical electromechanical relations can be written using the following ODEs:

$$L\dot{I}_m + RI_m = V_{in} - \varepsilon_b \tag{1}$$

$$J\dot{\omega}_m = T_m \tag{2}$$

where $I_m, V_m,$ and ε_b denote the motor's electrical current, voltage, and back-emf, respectively. The mechanical torque, T_m, is obtained from the motor's electrical current via the static relation:

$$T_m = k_T I_m \tag{3}$$

and the electrical back-emf is obtained from the motor's angular velocity via

$$\varepsilon_b = k_B \omega_m \tag{4}$$

Substituting the torque and back-emf of Eqs. (3) and (4) into the motor's dynamical equations (Eqs. (1) and (2)), and performing the Laplace transform with zero initial conditions yields:

$$(Ls + R)I_m(s) = V_{in}(s) - k_B \omega_m(s) \tag{5}$$

$$Js\omega_m(s) = k_T I_m(s) \tag{6}$$

From Eq. (6), I_m can be written as $I_m(s) = \frac{Js}{k_T}\omega_m(s)$, after substitution of I_m into Eq. (5), the relation between the motor's input voltage, V_{in}, to its angular velocity, ω_m, is obtained as:

$$\omega_m(s) = \frac{k_T}{JLs^2 + JRs + k_B k_T} V_{in}(s) \tag{7}$$

Since the motor's angular position, θ_m, is obtained by integrating its angular velocity, the transfer function from the motor's input voltage to its angular position, $G_1(s)$, can be written as:

$$G_1(s) = \frac{1}{s}\frac{k_T}{JLs^2 + JRs + k_B k_T} \tag{8}$$

Such that the following relation holds $\theta_m(s) = G_1(s)V_{in}(s)$.

Following the assumptions above, the free three DOF structure's equations of motion (EOM) can be written using matrix notation as:

$$\begin{bmatrix} m & 0 & 0 \\ 0 & m & 0 \\ 0 & 0 & m \end{bmatrix}\begin{bmatrix} \ddot{q}_1 \\ \ddot{q}_2 \\ \ddot{q}_3 \end{bmatrix} + \begin{bmatrix} 2c & -c & 0 \\ -c & 2c & -c \\ 0 & -c & c \end{bmatrix}\begin{bmatrix} \dot{q}_1 \\ \dot{q}_2 \\ \dot{q}_3 \end{bmatrix} + \begin{bmatrix} 2k & -k & 0 \\ -k & 2k & -k \\ 0 & -k & k \end{bmatrix}\begin{bmatrix} q_1 \\ q_2 \\ q_3 \end{bmatrix} = \begin{bmatrix} 0 \\ 0 \\ 0 \end{bmatrix}. \tag{9}$$

Since we assumed that the lead screw is infinitely rigid, it follows that $q_1 = d = p\theta_d$. After substituting q_1 into the EOM of Eq. (9), and moving all terms concerned with θ_d to the equations' right-hand side, the following set of equations is obtained:

$$\begin{bmatrix} m & 0 \\ 0 & m \end{bmatrix}\begin{bmatrix} \ddot{q}_2 \\ \ddot{q}_3 \end{bmatrix} + \begin{bmatrix} 2c & -c \\ -c & c \end{bmatrix}\begin{bmatrix} \dot{q}_2 \\ \dot{q}_3 \end{bmatrix} + \begin{bmatrix} 2k & -k \\ -k & k \end{bmatrix}\begin{bmatrix} q_2 \\ q_3 \end{bmatrix} = \begin{bmatrix} c \\ 0 \end{bmatrix} p\dot{\theta}_d + \begin{bmatrix} k \\ 0 \end{bmatrix} p\theta_d. \tag{10}$$

The transfer function from θ_d to q_3 can be obtained by taking the Laplace transform of Eq. (10) assuming zero initial condition, so that:

$$\begin{bmatrix} ms^2+2cs+2k & -cs-k \\ -cs-k & ms^2+cs+k \end{bmatrix} \begin{bmatrix} q_2(s) \\ q_3(s) \end{bmatrix} = \begin{bmatrix} 1 \\ 0 \end{bmatrix} (cs+k)p\theta_d(s) \tag{11}$$

Multiplying by the inverse of the left-hand-side matrix results in

$$\begin{bmatrix} q_2(s) \\ q_3(s) \end{bmatrix} = \frac{cs+k}{m^2s^4+3cms^3+(c^2+3km)s^2+2cks+k^2} \begin{bmatrix} ms^2+cs+k \\ cs+k \end{bmatrix} p\theta_d(s) \tag{12}$$

Denoting the transfer function from $\theta_d(s)$ to $q_3(s)$ as $G_2(s)$ such that $q_3(s) = G_2(s)\theta_d(s)$ it follows, based on Eq. (12), that $G_2(s)$ is equal to:

$$G_2(s) = \frac{c^2s^2+2cks+k^2}{m^2s^4+3cms^3+(c^2+3km)s^2+2cks+k^2} p \tag{13}$$

Figure 4 shows the frequency response of the electrical motor (G_1) and the 3 DOF system (G_2) for the physical values used in the simulation, which are given in Table 1.

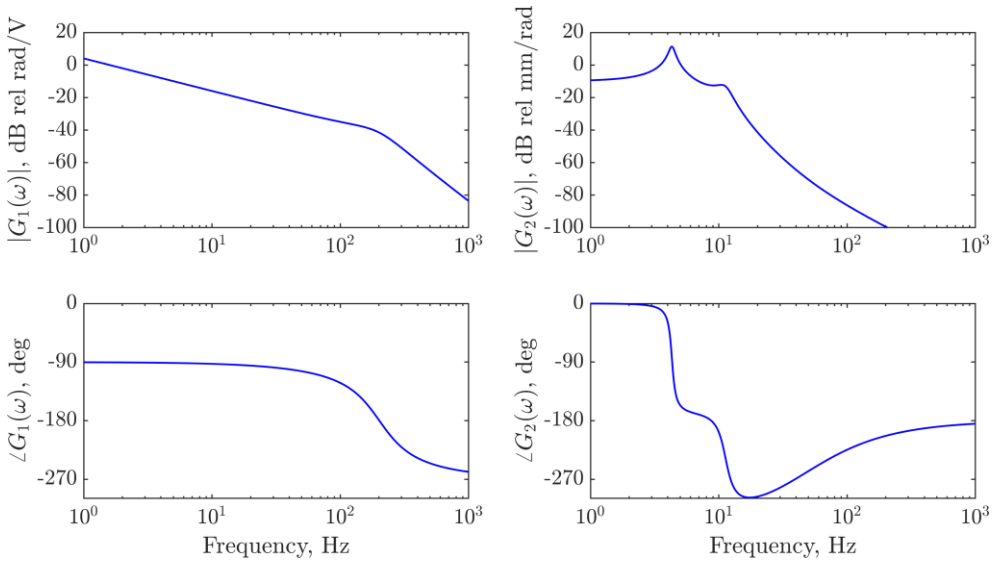

Figure 4 – Frequency response of the two linear parts of the plant.

Table 1 – Physical properties and values used in the numerical simulation of the three DOF with the DC electrical motor.

Symbol	Description	Value, units
$\boldsymbol{m}$	The lumped platform's mass	5.2, kg
$\boldsymbol{k}$	The beam's equivalent stiffness coefficient	$1 \cdot 10^4$, N/m
$\boldsymbol{c}$	The beam's equivalent damping coefficient	36.9, N/(m·s)
$\boldsymbol{J}$	The lumped motor's inertia	$5 \cdot 10^{-6}$, kg·m^2
$\boldsymbol{p}$	The lead screw pitch	$10^{-3}/2\pi$, m/rad
$\boldsymbol{L}$	The electrical motor's lumped inductance	$1 \cdot 10^{-3}$, H
$\boldsymbol{R}$	The electrical motor's lumped resistance	12, ohm
$\boldsymbol{k_T}$	The electrical motor's torque gain	0.8, (N·m)/A
$\boldsymbol{k_B}$	The electrical motor's back-emf gain	0.1, V/(m/s)

2.2. Linear control formulation

Since the open-loop transfer function (which at this stage is given by $G_1 G_2$) contains an integrator. A feedback controller is needed to obtain the desired steady state response. Additional potential advantages of using a feedback-loop are the ability to generate a closed loop response that is relatively insensitive to changes in the dynamical behaviour of the open-loop system, and the ability to attenuate disturbances and noise measurements on the system response.

A filtered PID (PIDF) controller is designed for the feedback system, using MATLAB's *pidtune*() function. The PIDF has the following structure:

$$C_{PIDF}(s) = K_p + K_i \frac{1}{s} + K_d \frac{s}{T_f s + 1} \tag{14}$$

where K_p, K_i, and K_d are the proportional, integral, and differential gains, respectively, and T_f is the differential filter time constant. The requirements used in the controller's design are zero steady-state error, a bandwidth frequency of 10 rad/sec, and a minimum phase margin of 10 deg. For these requirements, the controller constants given by *pidtune*() are: $K_p = 1377.7, K_i = 18907.6, K_d = -135.1,$ and $T_f = 0.1$.

Although, in principle, a filtered PD controller can achieve the first requirement (due to the integrator in G_1) it does not achieve the required bandwidth. In addition, a PD controller will be more sensitive to disturbances, and so an integrator was included in the controller.

Figure 5 shows the step and frequency responses of the linear closed-loop feedback system from the reference signal, r, to the position of the top mass, which is the output signal, y, given by:

$$G_{cl}(s) = C_{PIDF}(s)G_1(s)G_2(s)/\big(1 + C_{PIDF}(s)G_1(s)G_2(s)\big). \quad (15)$$

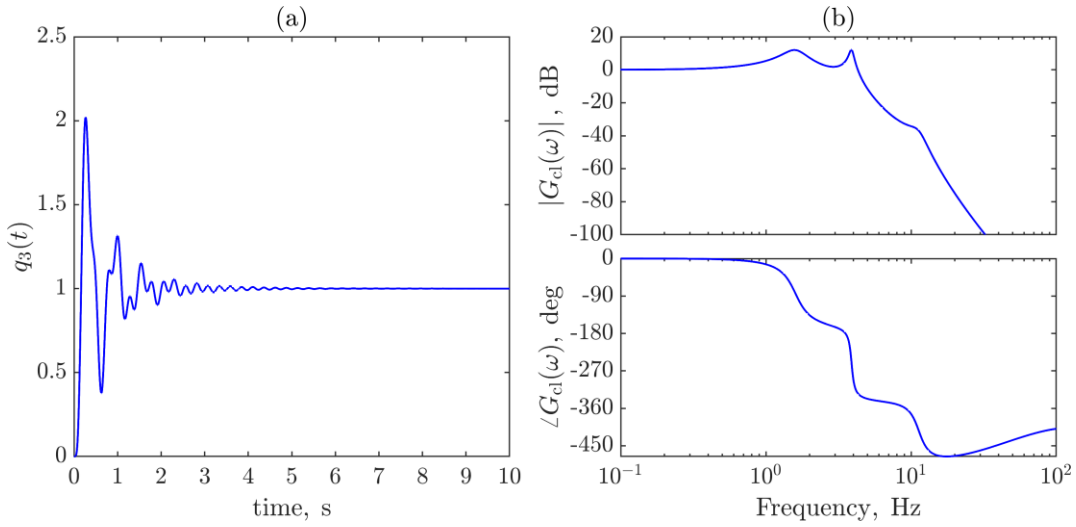

Figure 5 – The closed-loop top mass's step response (a), and the closed-loop frequency response (b).

There are two significant resonances in the closed-loop frequency response, and transients from both of these can be seen in the step response. This resonance frequency must be kept high to obtain the desired bandwidth. The resonances are also not highly damped, so that both overshoot and decaying residual vibrations are seen in the step response. However, the overshoot level and the settling time are acceptable based on the control requirement.

3. Backlash and its effect on the control

The worm gear's backlash mechanism is modelled as a shifted dead zone. Each time the rotation direction changes, a new dead zone of a given backlash gap angle begins. The backlash can be modelled using the state diagram presented in Figure 6.

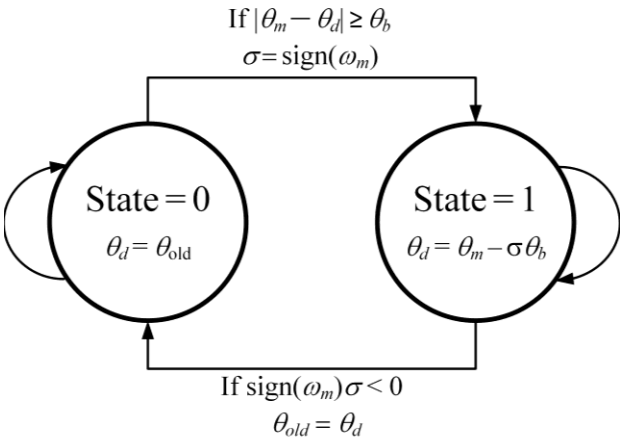

Figure 6 – Backlash model state diagram.

The backlash gap angle, or width, is defined as θ_b, its inputs are θ_m and ω_m, and its output is θ_d. In the state-diagram θ_{old} represents the last value of θ_d for the backlash function before it enters the gap, sign denotes the Signum function, where $\sigma = \text{sign}(\omega_m)$ denotes the direction of rotation after the backlash is transverse. When the backlash is closed, State 1 in the state diagram, the lead screw angle is equal to that of the motor minus the gap, i.e.,

$$\theta_d = \theta_m - \sigma\theta_b \tag{16}$$

where θ_b is the backlash gap angle. When the motor direction of rotation is switched, which is given mathematically as:

$$sign(\omega_m)\sigma < 0 \tag{17}$$

the lead screw has to transverse the backlash gap again, State 0 in the state diagram, and θ_d remains constant until the gap is closed, i.e., until the following is being satisfied:

$$|\theta_m - \theta_d| \geq \theta_b \tag{18}$$

In Eq. (18) the larger than function is used to avoid numerical errors. However, in reality, once the equality criterion is obtained, the difference between the two angles will remain constant.

If the backlash angle were constant, the backlash block could be used in a *Simulink* simulation. Since the backlash angle changes with time, however, a separate program for the state transitions had to be written, as below. To illustrate its response, Figure 7 shows the output of the backlash mechanism for the case where $\theta_b = 20$ deg, and for the following input:

$$\theta_m(t) = (1 + t/10)sin\,(2\pi t) \tag{19}$$

The lost motion between θ_m and θ_d can be seen in Figure 7(a), which shows their two waveforms, whereas the nonlinear characteristics of the backlash are more transparent in Figure 7(b), which plot one against the other.

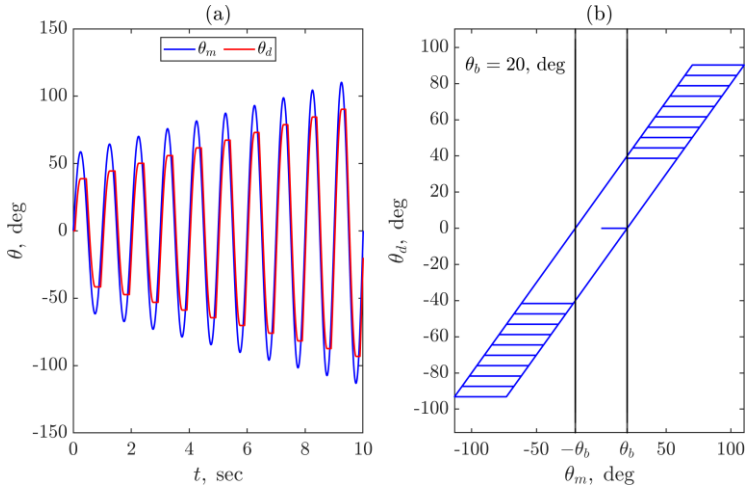

Figure 7 – The backlash model's input and output for the excitation given in Eq. (19), in terms of the individual waveforms of θ_m and θ_d (a), and the nonlinear characteristic of one against the other (b).

3.1. Effect of the backlash on the feedback-controlled system

To simulate the effect of backlash on the feedback control loop, the block diagram of Figure 3 was modified by introducing the backlash between the two dynamic plants, G_1 and G_2, as shown in Figure 8.

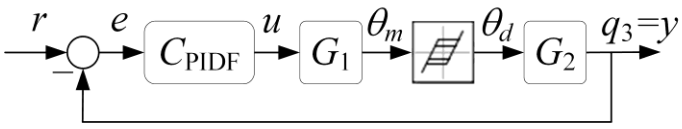

Figure 8 – The block diagram of the closed-loop system with the modelled lead screw's backlash.

The resulting step response of the feedback system, with the PID controller designed above, for different backlash angles is shown in Figure 9(a), whereas Figure 9(b) shows the electrical motor's angle, θ_m, and the lead-screw's angle, θ_d.

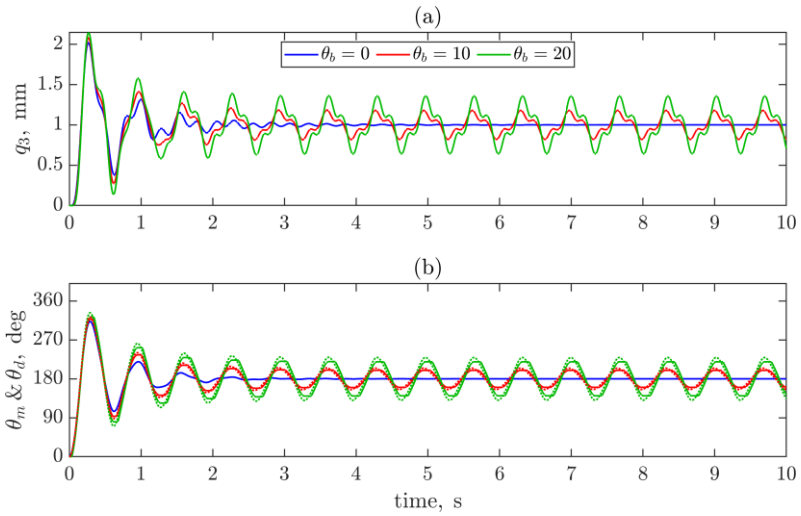

Figure 9 – The top platform position for different backlash angles (a), the lead screw's angle(solid line), and motor's angle (dashed line) for the corresponding backlash angle (b). Both subplots share the legend.

The simulation results presented in Figure 9 show that when backlash is present, the steady-state response exhibits a limit cycle and so is not asymptotically stable. Furthermore, the limit cycles' amplitude increases

with the backlash angle. Therefore, a nonlinear controller will be described in the following section that can be used to stabilise the feedback system when backlash is present.

3.2. Dead zone anti-backlash controller

The dead zone aims to avoid the limit cycle oscillations caused by the backlash by implementing feedback control only when the system's output is significantly different from the required command signal and opening the feedback loop if the error between these two signals is smaller than a given tolerance. By doing so, the control effectively implements a minimal control effort in the backlash gap, which is the preferred strategy for dealing with backlash in feedback loops [7]. However, the system does not stop instantaneously when the feedback loop is opened, and inertial effects will still occur. As a result, if the dead zone's tolerance is chosen to be too small compared with the backlash gap, the inertial effects will be dominant, and the limits cycles will remain (although with a different phase, amplitude, and even frequency). The three DOF system, G_2, is asymptotically stable. Therefore, if the error enters the dead zone without enough inertia to get out, it will remain inside it, and the oscillation will decay away until a steady state value is reached. However, this steady state value is, most likely, biased compared to the reference value. Thus, it should be possible to restabilise the system in the presence of backlash with a dead zone anti-backlash controller (referred to herein as a DZ controller). The design of the dead zone is a trade-off between avoiding a limit cycle oscillation and generating too significant a difference between the output and the command signal and increasing the settling time.

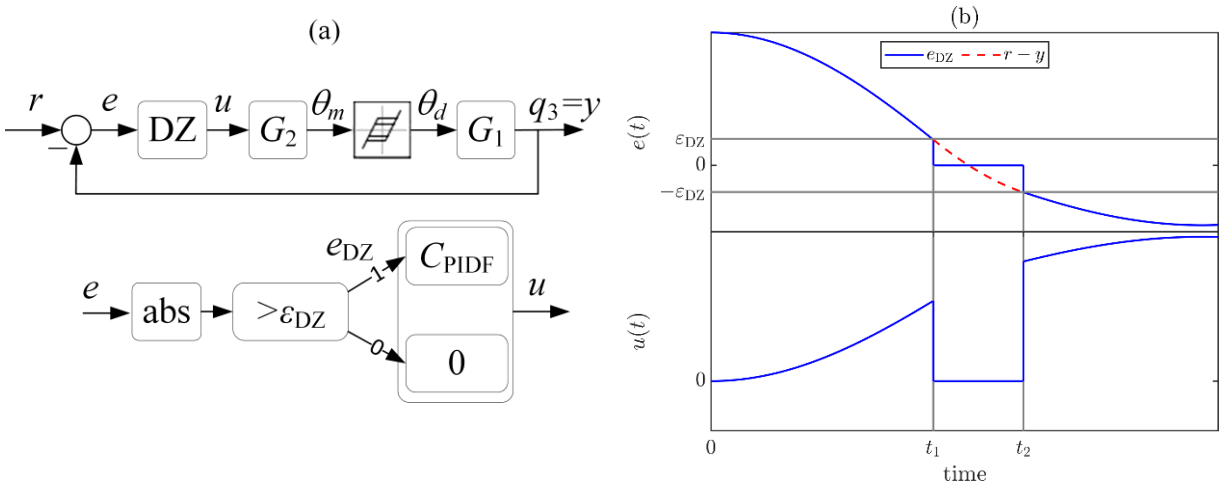

Figure 10 – The block diagram of the nonlinear plant and the proposed anti-backlash controller (a), and an example of the DZ controller signals and switching (b).

Figure 10(a) shows the block diagram of the nonlinear DZ controller, as well as the nonlinear plant with backlash between the angle of the motor, θ_m, and the lead screw θ_d. The control signal, u is now either the current output of the C_{PIDF} controller or zero, depending on whether the error is outside or inside the required tolerance. A dead zone error, which drives the controller, is also introduced to avoid changing the integrator part of the controller within the dead zone. The dead zone error is denoted as e_{DZ} and follows the following switching rule:

$$e_{DZ}(t) = \begin{cases} e(t) & |e(t)| > \varepsilon_{DZ} \\ 0 & |e(t)| \leq \varepsilon_{DZ} \end{cases} \tag{20}$$

Where $\varepsilon_{\mathrm{DZ}}$ denotes the dead zone tolerance. In the current work $\varepsilon_{\mathrm{DZ}}$ is associated with the estimated backlash angle, $\hat{\theta}_b$, via the pitch p and the DZ gain k_{DZ}, such that

$$\varepsilon_{DZ} = k_{DZ} p \hat{\theta}_b \tag{21}$$

The DZ gain is assumed to be constant in these simulations, with a value of unity, but generally could be made a function of $\hat{\theta}_b$. A direct result of this switching law is that the closed-loop feedback is only used when the top mass position is more than a certain distance from the required position, and the motor remains undriven when the output position is close to that required. Therefore, the system dynamics can

be represented by a state-dependent switching law. When the error is large, the dynamics are described by the closed feedback loop G_{cl}, driven by the error signal. When the error is small, the dynamics are described by the initial condition (zero-input) behaviour of the open-loop systems: G_1, the backlash, and G_2. The system is now nonlinear due to both the backlash and the switching. Therefore, its stability and performance depend on several factors, such as the reference amplitude, backlash angle, and the dead zone tolerance.

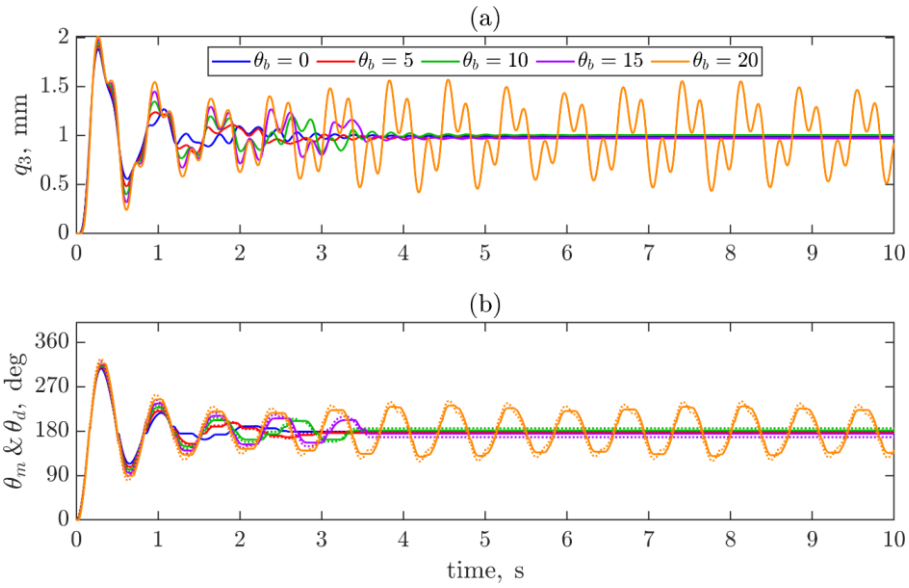

Figure 11 – The top platform position for different backlash angles (a), the lead screw's angle (solid line) and motor's angle (dashed line) for the corresponding backlash angle (b). Both subplots share the legend.

Figure 11 shows the step response simulation results of the feedback system with a dead zone anti-backlash controller. Different values of backlash were considered, with a DZ controller having a fixed value of dead zone error, $\varepsilon_{\mathrm{DZ}}$, to examine the mismodel effect between the estimated and the actual backlash angles. The estimated backlash angle was set to be $\hat{\theta}_b = 10$ deg. The DZ gain was chosen as unity, $k_{\mathrm{DZ}} = 1$, and the effect of this parameter on stability and performance remains an open question for the moment. From the results shown in Figure 11 it can be seen that the DZ controller restabilises the feedback system when the backlash angle is 0, 5, 10 or 15 degrees. If the backlash angle is an over-estimate, i.e., $\hat{\theta}_b > \theta_b$, the

feedback system is stable in these simulations, but the steady state bias is changed. The dependency of the bias on the estimation error is not transparent, however. For an under-estimate of the backlash angle, i.e., $\hat{\theta}_b < \theta_b$, the feedback system remains stable up to some limiting value. The identification of the backlash-angle thus does not need to be exact in order for the dead zone to stabilise the system. However, if the estimator is chosen "conservatively" to be somewhat larger than required, then the system will be open-loop for a large band of errors and so will be more sensitive to disturbances. Therefore, only an "accurate enough" estimation of the backlash angle is required in the controller.

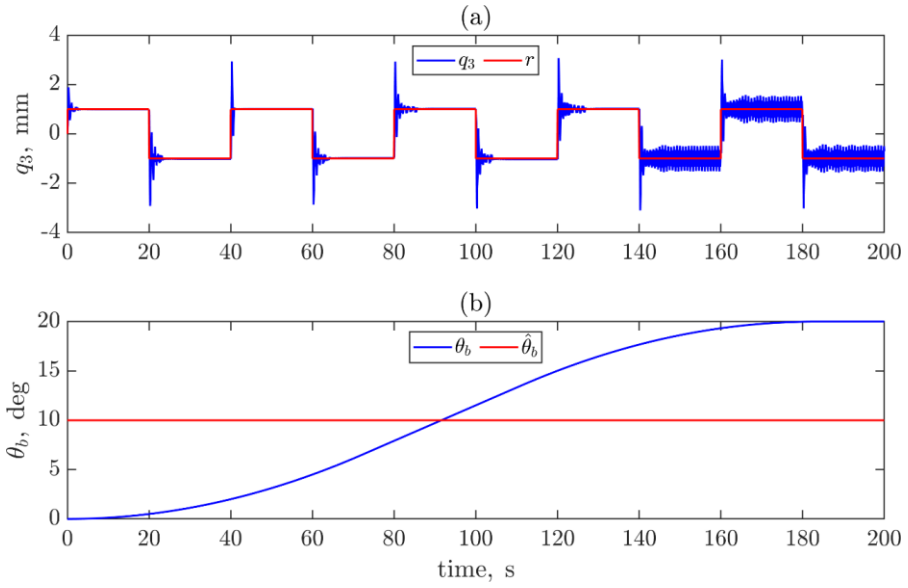

Figure 12 – The top platform position, q_3, the reference signal, r (a), and the actual and estimated backlash angles (b).

Figure 12 shows simulation of the response with a square-wave command signal for the feedback system with a time-varying backlash angle and constant estimated backlash angle, with a DZ controller having a fixed value of $\varepsilon_{\mathrm{DZ}}$. The simulation was carried out to illustrate the effect of changes in the backlash angle. The command signal used throughout the simulation, shown in Figure 12(a) (Red solid line), is a square wave with a 1 mm amplitude. Based on the transient settling time of the linear system, the period of the square wave was set to 40 seconds so that the transient response had substantially decayed before the following change in the command signal. A time-varying backlash is now assumed, which changes

according to an S-curve profile over 200 seconds, as shown in Figure 12(b) (Blue solid line), representing a highly accelerated wearing process. A constant estimated backlash angle, $\hat{\theta}_b = 10$ deg, was, however assumed in the simulation to set $\varepsilon_{\mathrm{DZ}}$. The command and output signal of the simulation are shown in Figure 12(a), and the actual and estimated backlash angles are shown in Figure 12(b). Note that stability is lost when the actual backlash angle becomes significantly larger than the estimated one used to set the $\varepsilon_{\mathrm{DZ}}$ parameter in the dead zone, 17 degrees compared to 10 degrees in this case.

Based on these simulations, the need to update the backlash estimator is apparent when the backlash changes over time. Therefore, in the following section, a use of a digital twin is discussed in order to update the estimation of the backlash angle.

4. Digital twin with backlash identification and closed-loop simulations

The simulation's results presented in Section 3.2 illustrate the importance of having an "accurate enough" estimation of the current backlash angle. A digital twin is now employed to estimate the backlash angle and hence reconfiguration of the controller. The digital twin is assumed to be implemented remotely, as in Figure 1, to avoid an over-complicated real-time controller design around the physical twin. The digital twin used in these simulations does not aim to mimic a fully operational one. Instead, only the digital twin's systems' models and communication capabilities are considered. This highlights how the digital twin can be used in real-time model estimation and controller reconfiguration without venturing into the discussion of what encompasses a digital twin.

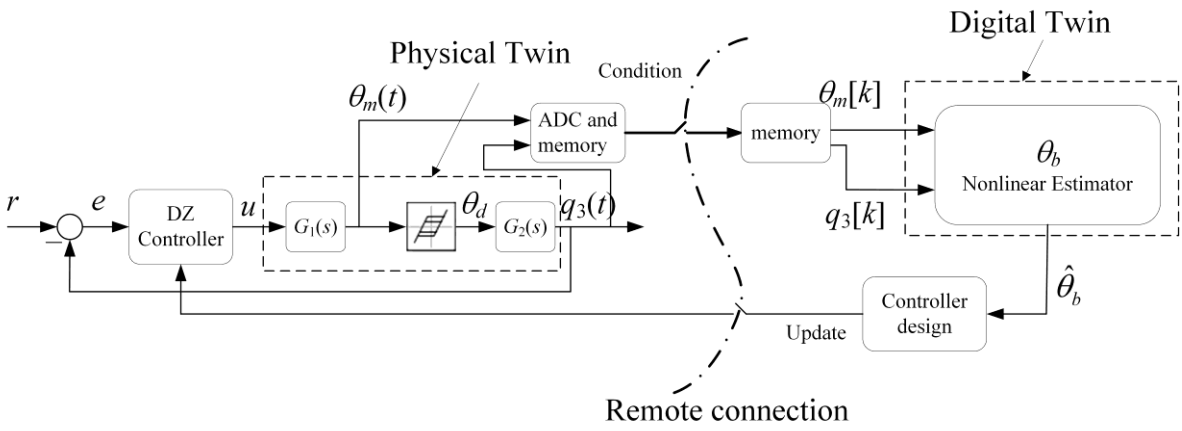

Figure 13 – The block diagram of the physical-digital twin configuration used in Section 4 simulations.

The detailed physical arrangement is shown in Figure 13, in which the controller is implemented in real-time, while the updating processes that require extensive signal processing, including the implementation of the digital twin, take place on a remote machine. The left-hand side of the diagram of Figure 13 represents the physical twin, and the right-hand side is the digital one. The physical twin comprises the dynamic plants, the DZ controller, and a data acquisition system operating in real-time. The right-hand side of the diagram shows the digital twin, which realises the various filters and the backlash angle nonlinear estimator and uses this estimation to update the DZ controller. The remote connection enables passing the measured data between the two at discrete well separated events and updating the dead zone parameter. The relevant system states of the real-time control loop, which are the measured motor angle, θ_m, and the top platform position, q_3, are stored in temporary memory and sent to the digital twin using an asynchronous interface connection. In the current configuration, it is assumed that the digital twin runs once after each change of the reference signal (after the buffer is full). An unknown delay may be introduced due to the nature of this interface. The states are recorded in a local buffer, the contents of which are sent to the digital twin at each update time instance. The overall delay in the transmission is thus the sum of the buffer data acquisition time and the communication and data transfer times. While the latter, in general, is a non-deterministic quantity, the intersample delay between consecutive samples within the buffer is both constant and known. Based on the digital twin decision, the dead zone parameter in the real-

time controller can be reconfigured to ensure the system's stability. More sophisticated controller re-design methods could also be envisaged, which may involve running multiple digital twin simulations at a fast simulation rate compared to real-time and tuning the PID parameters as well, for example.

If a microcontroller is used to implement the sampling and data storage functions on the left-hand side of Figure 13, it may well have enough processing power also to implement a novelty detection system [24], instead of updating based on the reference signal. This can be used to ensure that the state variables are only transmitted to the digital twin once a significant change in the backlash is detected and reduce the overall time and communication resources.

A simplified form of a digital twin is used here to demonstrate its use in the reconfiguration of the controller. The right-hand part of Figure 13 shows the block diagram of the digital twin, which has dynamical models of sub-systems, G_1 and G_2, in the form of their transfer functions. It is assumed that G_1 and G_2 are modelled accurately, based on a preliminary linear identification procedure [16]. The current work also assumes that these linear systems parameters are constant in time, unlike the backlash angle. This assumption depends on the application and the different timescale of the wear responsible for changing the backlash angle and other processes that might change the system's mass or stiffness.

It is assumed that the motor's angle, θ_m, and the top platform position, q_3, are measured at a sampling rate of 5 kHz, and the buffer size is chosen to correspond to one second of measurement time, resulting in a total of $10{,}000$ samples for both signals. It is also assumed that the local controller and the digital twin's server are connected via a local router. Therefore, the end-to-end delay is the sum of the processing, queuing, transmission and propagation delays [25]. In modern routers configured to simple packet forwarding, processing delays are of the order of microseconds and can be neglected [25,26]. If the router is used only for the communication between the controller and server, and the packet's transmission ends before the next one is received, the queuing delay is zero. Assuming a data transfer rate of 100 Mbits, and 16 bits data, the communication time delay between the physical to the digital twin has a delay of 1.6 ms.

Finally, the propagation delay of a local network is also on the order of microseconds and is, therefore, negligible.

To conclude, the end-to-end time delay in the current work is equal to the transmission delay and a small, positive-valued uncertainty on the order of milliseconds. Therefore, a 1-second delay was added, in addition to the inherent buffer delay, for each communication channel in the current simulation. The added delay also ensures that the estimation algorithm will converge before sending the new estimation.

The digital twin uses its knowledge of the different elements to estimate the motor's and lead screw's angles from the measured signals and consequently estimates the current backlash angle. The estimated backlash angle is then used to set the extent of the dead zone when updating the controller. The estimation method used for the lead screw's angle is described first in Section 4.1. Then, the simulated physical and digital twin results are discussed for the time-varying backlash angle in Section 4.2. Finally, the case of noisy measurements is discussed in Section 4.3.

4.1. Backlash angle estimation

After each data transmission, the digital twin can be used to simulate the internal signals of the feedback system. However, since the communication is event-based, and only a partial time history is available for the digital twin, it is necessary to estimate internal signals without accurate knowledge of their initial conditions. The approach used here is based on a linear observer, which can overcome the uncertainty in the initial conditions and be combined with a nonlinear optimiser to estimate the backlash gap angle and the lead screw initial angle.

An angular position sensor is used to measure θ_m directly, and so avoid the use of the estimated motor dynamics; however, if the motor's position is not accessible, the initial conditions (angular position and velocity) can be added as additional parameters to the nonlinear optimiser. The output of the backlash, the lead screw's angle, is estimated using the backlash model of Section 3, although, in the sampled version of the model, the sign of the motor's angular velocity is estimated using a first-order finite-difference.

The optimisation goal is formulated as follows: Given a model of the 3 DOF structure dynamics in terms of its transfer function, $G_2(s)$, a set of measurements, $\theta_m[k] = \theta_m(t_0 + kT_s), q_3[k] = q_3(t_0 + kT_s), k = 0, \dots, N-1$, where T_s denotes the sampling time, and a discrete backlash model with input θ_m and output θ_d, given by

$$\theta_d[k] = B(\theta_b, \theta_m[k], \theta_m[k-1], \theta_d[k-1]), k = 1, \dots, N-1 \quad (22)$$

Then by defining $\hat{q}_3(t_0 + kT_s)$ as the estimator output, and $\hat{\xi}_3(t_0 + kT_s)$ as the estimator residual, we would like to minimise the steady-state squared rms of the estimator residual $\left(\hat{\xi}_3\right)$:

$$\min_{b,w_0} \sum_{k=k_s}^{N-1} \left(\hat{\xi}_3(t_0 + kT_s)\right)^2 = \min_{b,w_0} \sum_{k=k_s}^{N-1} \left(q_3(t_0 + kT_s) - \hat{q}_3(t_0 + kT_s)\right)^2 \quad (23)$$

The minimisation problem should be an unbiased estimator, meaning that when the backlash output and the backlash output initial condition are known accurately, b^* and w_0^*, the $\hat{\xi}_3$ rms is at a global minimum. However, in the current formulation, there are no additional constraints imposed on G_2. Expressly, we do not assume the knowledge of its initial conditions, and the effect of these initial conditions in the steady state could lead to a biased estimation.

To ensure that the minimiser is unbiased, a linear state estimator, whose structure is described in the Appendix, is put forward to eliminate the effect of the initial conditions. The weight vector of the linear estimator is chosen to attenuate the linear estimation error in less than $k_s T_s$ seconds.

The nonlinear estimator block diagram is presented in Figure 14. The solution to the nonlinear minimisation problem could be obtained by employing a variety of known minimisation algorithms on the digital twin, which can simulate the estimator much faster than real-time. In this work, the unconstraint BFGS Quasi-Newton method with cubic line search was chosen to solve the optimization problem. The initial conditions for the nonlinear minimiser were chosen to be the previous backlash angle and the first sample of the motor's angle minus the prior backlash angle multiplied with a forward finite difference estimation of the motor's direction.

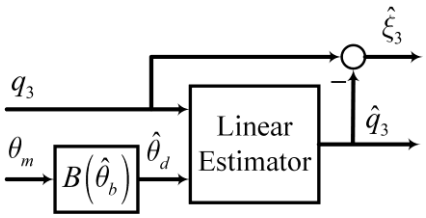

Figure 14 – The nonlinear estimator block diagram.

4.2. Simulation of a digital twin based reconfigurable controller

A *Simulink* and *MATLAB* simulation was used to validate the proposed control scheme. The physical twin, sensors, buffers, and communication were realised in the *Simulink* environment, and the digital twin nonlinear optimisation was realised using a *MATLAB* function. In addition to the buffer delay, a 1-second delay was added to each communication between the digital and physical twin, representing an upper bound on the possible communication delay and the time the digital twin takes to solve the optimisation problem. The reference signal and the backlash angle profile used for the current simulation are the same as the previous simulation (Section 3.2). The controller parameters were kept the same with $k_{\mathrm{DZ}} = 1$. The parameters of the digital twin post-processing were chosen as: $\mathrm{N} = 2, \varepsilon_{\mathrm{d}} = 0.1\ \mathrm{rad/s}$, and $l = 1/10$. The initial backlash estimator was set to zero ($\hat{\theta}_b(0) = 0$), and the lead screw's angle initial position was set to the middle of the backlash.

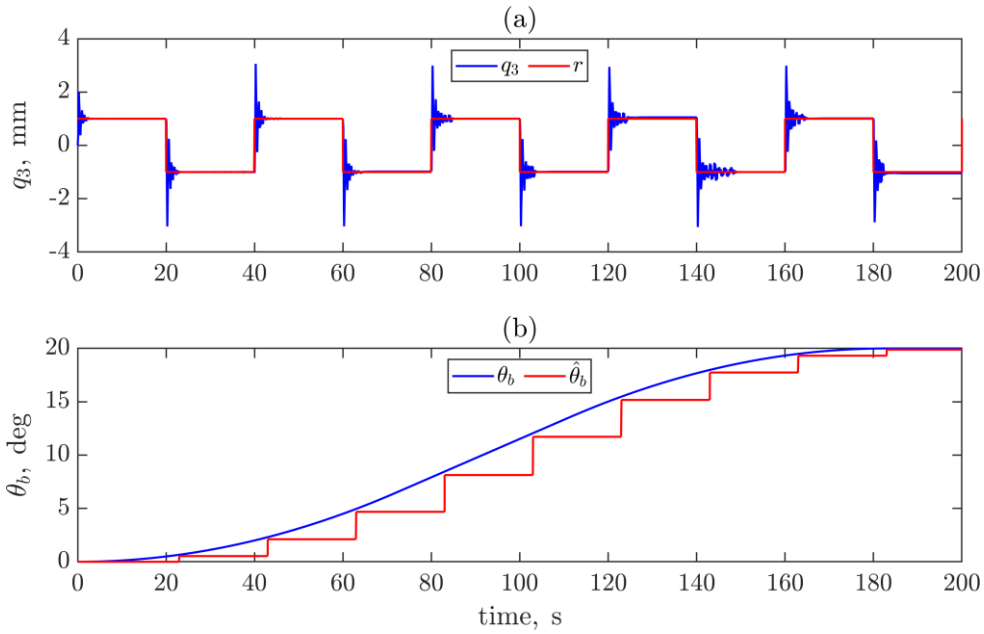

Figure 15 – Top platform position, q_3, the reference signal, r (a), and the actual and estimated backlash angles (b).

Figure 15 shows the simulation results of the digital twin based reconfigurable controller simulation with a time-varying backlash angle. Note that unlike the previous simulation results (Figure 12), the reconfigurable controller now restabilises the nonlinear feedback system at all times. Compared with the result in Figure 5(a), the settling time is increased by the communication and estimation delay. Since the backlash is assumed to change unrealistically fast in these simulations, the estimator needs to change constantly, but in more realistic scenarios, the estimator would only be required occasionally. Even though a bias in the final position of each step is present, the worst bias is under 5% of the required reference amplitude. The lead screw's angle estimation procedure is seen to yield a sufficiently accurate estimation for stable control.

The introduction of a digital twin enables us to restabilise the system when it is subject to a nonlinear, nonstationary backlash mechanism. This was achieved without changing the structure of the simple PID-based dead zone controller.

4.3. Simulation of a digital twin based reconfigurable controller with measurement noise

It is important in practice to also consider the case of non-ideal sensors and a noisy environment. Uncorrelated filtered Gaussian noise was added to the measured top platform's position, which altered the tracking error used in the feedback controller. The noise power was set to represent a realistic measurement scenario, with a standard deviation of 0.22mm, about a quarter of the size of steps in the reference signal or an SNR of 20dB. Both the measured motor's angle and top platform position were passed through a noncausal lowpass (with a zero-phase shift) filter in the digital twin. The filtered signals were then used as the inputs of the nonlinear optimisation. The feedback loop was modified to include a first-order lowpass to filter the measured top-platform position. The lowpass cut-off frequency was chosen to minimize the added phase lag near the structure resonances to ensure the closed-loop's stability.

The noise was created by passing a white noise generator through an IIR highpass filter with a stopband frequency of 10Hz, a passband frequency of 50Hz, and a minimum stopband attenuation of 40dB, thus mimicking the case where the noise spectrum is mainly concentrated at higher frequencies that the dynamical system spectrum. A 10^{th} order Butterworth filter was used for the noncausal filter, and both the lowpass filters were designed with the same cut-off frequency of 20Hz.

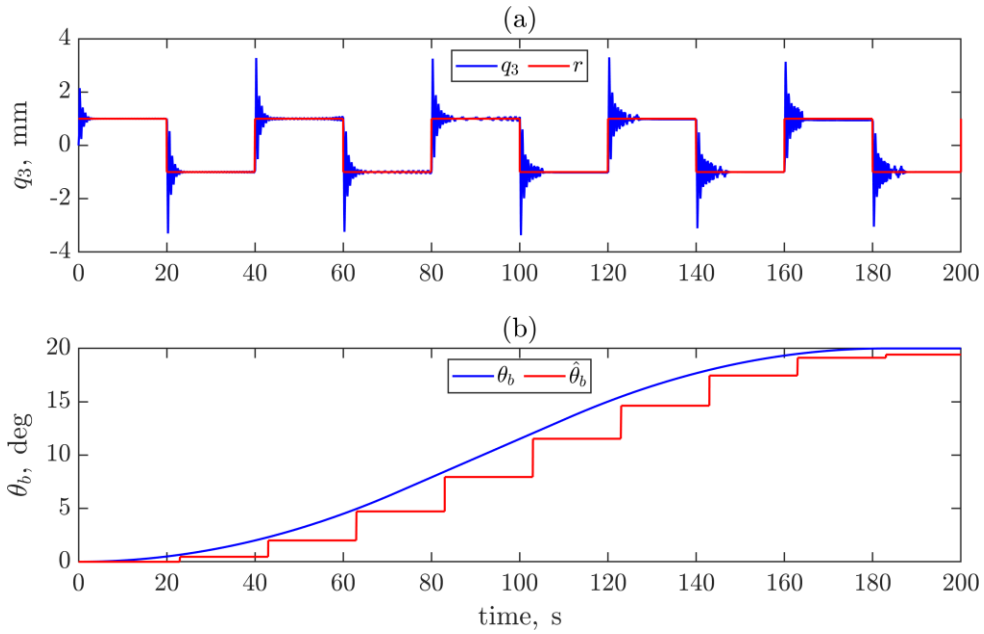

Figure 16 – The top platform position, q_3, the reference signal, r (a), and the actual and estimated backlash angles (b).

Figure 16 shows the simulation results of the digital twin based reconfigurable anti-backlash controller with an added 20dB SNR Gaussian measurement noise. The top platform position and not the noisy measurement of it is shown in Figure 16(a) since the noise and command signals' amplitudes are the same order of magnitude, making it hard to see the control action when looking at the noisy measurement. Based on Figure 16(b), it is noted that the backlash's angle estimation is now slightly biased since the noise is not filtered entirely from the measured noise. However, as shown in Section 3.2, only an approximated backlash estimation is needed to ensure stability, and so this does not alter the system performance, which is further supported by the response of the top platform shown in Figure 16(a).

The effect of noise on the linear controller (Figure 16(a) when time<20s) seems to be negligible, as expected. However, if a small dead zone is included in the controller, the noise in the feedback results in small amplitude steady state oscillations, as can be seen for the fourth and fifth steps (Figure 16(a) when 60s<time<100s). When the dead zone becomes larger, the effect of the noise diminishes. Therefore, another

possibility is to introduce a larger dead zone even for a small backlash gap's angle; this could be achieved by tuning the dead zone gain parameter, k_{DZ}, which is currently equal to unity.

Based on the result, it is seen that the proposed control scheme can cope with a realistically noisy environment and that the proposed estimation method, although slightly biased, is accurate enough to maintain control. If a very harsh environment with higher levels of noise is considered, both the controller and the estimation methods would need to be modified to incorporate a noise model.

5. Conclusions

Feedback controllers are widely used to control the position of dynamic systems but can perform poorly or become unstable if there are changes to the characteristics of the system under control. In this paper, a digital twin is used to track the changing behaviour of an example dynamic structure used in a position control system, for which the connection between the driving motor and the structure is subject to backlash, the extent of which changes over time. The dynamics of the example three degree of freedom structure and the motor are first modelled, and a PID controller is designed for this linear system. The controller's performance is then examined when there is an increase in the width of the backlash gap in the lead screw converting the rotation of the motor into the translational motion driving the structure. It is shown that the system can easily develop a limit cycle oscillation as the backlash gap increases. One method of suppressing these oscillations is to incorporate a dead zone into the controller, to ignore minor differences between the displacement of the structure and the command signal. The design of such a dead zone, which depends on the extent of the backlash, involves a trade-off between suppressing the oscillations and not incurring too large a steady-state error and an undesired long settling time.

A digital twin of the motor and structure is then used to estimate the extent of the changing backlash gap in the lead screw and hence alter the dead zone of the controller. More sophisticated implementations of the digital twin could also be envisaged, such as its use to also change the gain of the dead zone under different conditions, or the simultaneous identification of the motor and the dynamic system plants if they

were to change, but these avenues have not been explored here. Unlike the feedback controller, which needs to be local to the structure under control and operate in real-time, the digital twin, which requires considerably more processing power, does not need to be operating continuously. Therefore, the digital twin can be implemented remotely and only communicate with the physical twin via an asynchronous link with uncertain latency. Moreover, the digital twin can operate at rates much faster than real time to speed up the controller design. It is shown that by using the digital twin to track the changing backlash using nonlinear optimisation and hence retune the extent of the dead zone in the local controller, stability can be maintained when the backlash varies over a range for which a fixed dead zone would not give satisfactory performance. In these simulations, it is assumed that the digital twin is used regularly to estimate the extent of the backlash. However, it would also be possible to incorporate a novelty detector into the local controller and so only use the remote digital twin to retune the feedback if there was a significant change in the system under control.

Appendix – Linear state observer

A closed-loop state-observer [27] is used in the minimisation problem of Eq. (23), as shown in Figure 14. The state-observer inputs are the measured top platform's position, q_3, and the estimated lead screw's angle, $\hat{\theta}_d$, and its output is the estimated top platform's position $\hat{q}_3$, assuming zero-initial conditions.

The transfer function representation of the 3 DOF system, G_2, given in Eq. (13) can be written in a minimal observable canonical form state-space realisation as:

$$G_2(s) = C_o(sI - A_o)^{-1}B_o = \begin{bmatrix} A_o & B_o \\ C_o & 0 \end{bmatrix} = \begin{bmatrix} \begin{bmatrix} -a_3 & 1 & 0 & 0 \\ -a_2 & 0 & 1 & 0 \\ -a_1 & 0 & 0 & 1 \\ -a_0 & 0 & 0 & 0 \end{bmatrix} & \begin{bmatrix} 0 \\ b_2 \\ b_1 \\ b_0 \end{bmatrix} \\ \begin{bmatrix} 1 & 0 & 0 & 0 \end{bmatrix} & 0 \end{bmatrix} \quad \text{(A.1)}$$

where:

$$a_0 = k^2/m^2, a_1 = 2ck/m^2, a_2 = c^2/m^2 + 3k/m, and\ a_3 = 3c/m \quad \text{(A.2)}$$

and

$$b_0 = k^2 p/m^2, b_1 = 2ckp/m^2, and\ b_2 = c^2 p/m^2 \tag{A.3}$$

Using state-space notations and introducing the estimator gain vector L, the feedback state-estimator can be written as:

$$\begin{matrix} \dot{\hat{x}} = A_o\hat{x} + B_o\theta_d\ + L(q_3 - \hat{q}_3) \\ \hat{q}_3 = C_o\hat{x} \end{matrix} \Longrightarrow \begin{matrix} \dot{\hat{x}} = A_L\hat{x} + B_o\theta_d + Lq_3 \\ \hat{q}_3 = C_o\hat{x} \end{matrix} \tag{A.4}$$

Where $\hat{x}$ and $\hat{q}_3$ are the state vector and output estimators, and $A_L \equiv A_o - LC_o$. Assuming that no knowledge of the initial condition $x(0) = x_0$ is available, the linear observer error dynamics $\hat{e}_L = x - \hat{x}$ is dictated by the following homogeneous initial value problem

$$\dot{\hat{e}}_L = A_L\hat{e}_L, \hat{e}_L(0) = x_0 \tag{A.5}$$

Since the realisation is minimal, the matrix pair (A_0, C_o) is observable, and the poles of A_L can be assigned at will. By choosing the dominant mode settling time to be smaller than $k_s T_s$, the unknown initial condition dynamics no longer affect the nonlinear estimator.

One possible choice is to place all A_L eigenvalues at the same location, $-\alpha$. Leading to the following binomial expansion for the closed-loop characteristic polynomial:

$$\chi_L(s) = det(sI - A_L) = (s + \alpha)^4 = \sum_{i=0}^{4} \binom{4}{4-i} \alpha^i s^{4-i}, \binom{4}{4-i} = \frac{4!}{(4-i)!i!} \tag{A.6}$$

By writing the estimator gain vector as $L = [l_3 \quad l_2 \quad l_1 \quad l_0]^T$, it follows that the observer is also in the observable canonical form, and:

$$A_L = \begin{bmatrix} -(a_3 + l_3) & 1 & 0 & 0 \\ -(a_3 + l_2) & 0 & 1 & 0 \\ -(a_1 + l_1) & 0 & 0 & 1 \\ -(a_0 + l_0) & 0 & 0 & 0 \end{bmatrix} \tag{A.7}$$

Therefore, the observer characteristic polynomial is given by:

$$\chi_L(s) = s^4 + (a_3 + l_3)s^3 + (a_2 + l_2)s^2 + (a_1 + l_1)s + \ (a_0 + l_0) \tag{A.8}$$

Equating Eq. (A.6) and Eq. (A.8) results in the following choice of coefficients:

$$l_i = \binom{4}{4-i} \alpha^i - a_i \tag{A.9}$$

which ensures that the mode settling time is shorter than $k_s T_s$ by tuning α. Thus, by combining this linear state-observer with the tuned α and the nonlinear optimisation method described in Section 4.1, results in an unbiased estimation of the backlash gap.

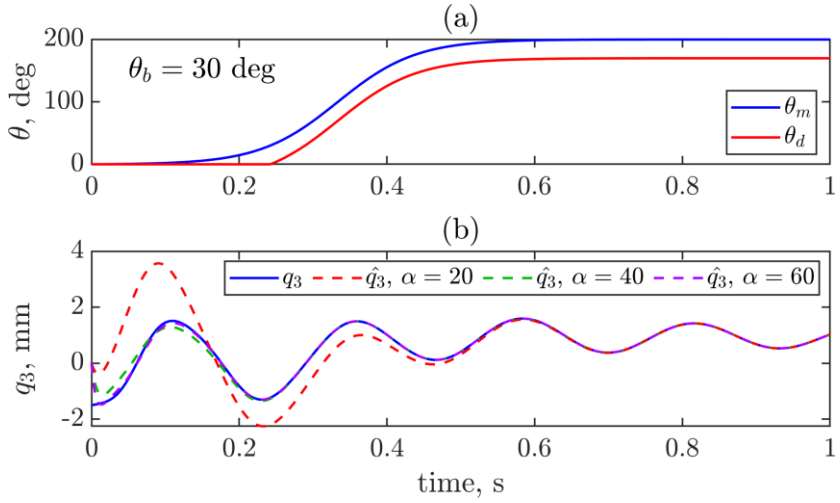

Figure A. 1 – The input motor's and lead screw's angle signals (a), and the electromechanical output for three different linear state-observers (b).

For example, Figure A. 1 shows a simulation of the estimation based on measurements obtained from G_2 assuming a backlash angle of 30 degrees, initial states of $[y_0, \dot{y}_0, \ddot{y}_0, \dddot{y}_0] = [-1.5,5,0.1,0] \cdot 10^{-3}$, and for different choices of the observer poles' location, α. The convergence time of the estimation depends on the selection of α. It can be noted based on Figure A. 1 that $\alpha = 40$ results in a good estimation of the output after 0.25sec, and therefore, it is used in the design of the digital twin.

Acknowledgement

The authors gratefully acknowledge the support of the UK Engineering and Physical Sciences Research Council (EPSRC) through the DigiTwin project (grant EP/R006768/1).

References

[1] K.J. Åström, B. Wittenmark, Adaptive control, Courier Corporation, 2013.

[2] D.J. Wagg, K. Worden, R.J. Barthorpe, P. Gardner, Digital Twins: State-of-the-Art and Future Directions for Modeling and Simulation in Engineering Dynamics Applications, ASCE-ASME J Risk Uncert Engrg Sys Part B Mech Engrg. 6 (2020). https://doi.org/10.1115/1.4046739.

[3] D. McLean, Automatic flight control systems, Prentice Hall, Englewood Cliffs, NJ, 1990.

[4] J.G. Njiri, D. Söffker, State-of-the-art in wind turbine control: Trends and challenges, Renew. Sustain. Energy Rev. 60 (2016) 377–393. https://doi.org/10.1016/j.rser.2016.01.110.

[5] J. Vörös, Modeling and identification of systems with backlash, Automatica. 46 (2010) 369–374. https://doi.org/10.1016/J.AUTOMATICA.2009.11.005.

[6] S. Villwock, M. Pacas, Time-domain identification method for detecting mechanical backlash in electrical drives, IEEE Trans. Ind. Electron. 56 (2009) 568–573. https://doi.org/10.1109/TIE.2008.2003498.

[7] M. Nordin, P.O. Gutman, Controlling mechanical systems with backlash—a survey, Automatica. 38 (2002) 1633–1649. https://doi.org/10.1016/S0005-1098(02)00047-X.

[8] L.E. Alban, Systematic analysis of gear failures, ASM International, 1985.

[9] G. Tao, P. V. Kokotovic, Adaptive control of systems with backlash, Automatica. 29 (1993) 323–335. https://doi.org/10.1016/0005-1098(93)90126-E.

[10] G. Tao, X. Ma, Y. Ling, Optimal and nonlinear decoupling control of systems with sandwiched backlash, Automatica. 37 (2001) 165–176. https://doi.org/10.1016/S0005-1098(00)00153-9.

[11] P. Rostalski, T. Besselmann, M. Barić, F. Van Belzen, M. Morari, A hybrid approach to modelling, control and state estimation of mechanical systems with backlash, Int. J. Control. 80 (2007) 1729–1740. https://doi.org/10.1080/00207170701493985.

[12] M.L. Corradini, G. Parlangeli, Robust stabilization of nonlinear uncertain plants with hysteresis in the actuator: A sliding mode approach, Proc. IEEE Int. Conf. Syst. Man Cybern. 3 (2002) 500–505. https://doi.org/10.1109/ICSMC.2002.1176093.

[13] D.R. Seidl, S.L. Lam, J.A. Putman, R.D. Lorenz, Neural Network Compensation of Gear Backlash

Hysteresis in Position-Controlled Mechanisms, IEEE Trans. Ind. Appl. 31 (1995) 1475–1483. https://doi.org/10.1109/28.475744.

[14] K.J. Åström, Advances in PID Control, 2018.

[15] D.J. Ewins, Modal testing: theory, practice and application, John Wiley & Sons, 2009.

[16] L. Ljung, System Identification, Prentice-Hall, Englewood Cliffs, NJ, 1987.

[17] S. Haykin, Neural networks: a comprehensive foundation, Prentice Hall, NJ, 1999.

[18] K. Worden, W.J. Staszewski, J.J. Hensman, Natural computing for mechanical systems research: A tutorial overview, Mech. Syst. Signal Process. 25 (2011) 4–111. https://doi.org/10.1016/j.ymssp.2010.07.013.

[19] P. Gardner, M. Dal Borgo, V. Ruffini, Y. Zhu, A. Hughes, Towards the Development of a Digital Twin for Structural Dynamics Applications, Conf. Proc. Soc. Exp. Mech. Ser. (2020) 165–179. https://doi.org/10.1007/978-3-030-47638-0_18.

[20] T. Chen, B.A. Francis, Optimal sampled-data control systems, Springer Science & Business Media, 2012.

[21] K.J. Åström, B. Wittenmark, Computer-controlled systems: theory and design, Courier Corporation, 2013.

[22] S.J. Elliott, Signal Processing for Active Control, Elsevier, 2001. https://doi.org/10.1016/b978-0-12-237085-4.x5000-5.

[23] M. Dal Borgo, P. Gardner, Y. Zhu, D.J. Wagg, S.K. Au, S. Elliott, On the development of a digital twin for the active vibration control of a three-storey structure, in: ISMA2020-USD2020 Proc., Leuven, Belgium, 2020.

[24] K. Worden, Structural fault detection using a novelty measure, J. Sound Vib. 201 (1997) 85–101. https://doi.org/10.1006/jsvi.1996.0747.

[25] J.F. Kurose, K.W. Ross, Computer networking: a top down approach, Pearson Education, Upper Saddle River, NJ, 2013.

[26] R. Ramaswamy, N. Weng, T. Wolf, Characterizing network processing delay, in: IEEE Glob. Telecommun. Conf. 2004. GLOBECOM '04., IEEE, 2004: pp. 1629–1634. https://doi.org/10.1109/GLOCOM.2004.1378257.

[27] K.J. Åström, R.M. Murray, Feedback Systems, Princeton University Press, 2010.